Supporting Information

Efficient methane to ethane conversion via C−H bond activation catalyzed by MOF-derived porous PdO/TiO_2 nanocomposite

Hai-Tao Wan,[a] Chang-Long Tan,*[b] Ming-Yu Qi,[b] Yin-Feng Wang,[a] Zi-Rong Tang*[a,b], and Yi-Jun Xu*[a,b]

[a] College of Chemistry, State Key Laboratory of Photocatalysis on Energy and Environment, Fuzhou University, Fuzhou 350116, P. R. China
[b] School of Materials and Energy & Institute of Fundamental and Frontier Sciences, University of Electronic Science and Technology of China, Chengdu 611731, P. R. China.
* To whom correspondence should be addressed.
E-mail: cl_tan@uestc.edu.cn; zrtang@uestc.edu.cn; yjxu@uestc.edu.cn

1. Materials

All the chemicals were used as received without further purification. The titanium ethoxide, 2,2'-bipyridine-5,5'-dicarboxylic acid (H_2BPDC), K_2PdCl_6, $HAuCl_4{\cdot}4H_2O$, $AgNO_3$, $H_2PtCl_6{\cdot}xH_2O$, $Cu(NO_3)_2{\cdot}3H_2O$, $Ni(NO_3)_2{\cdot}6H_2O$, Na_2SO_4, 5,5-Dimethyl-1-pyrroline-N-oxide (DMPO), P25, ZnO, CeO_2 and Al_2O_3 nanoparticles were purchased from Aladdin Company. The acetic acid, N, N-dimethylformamide (DMF), and ethanol were purchased from Tianjin Damao Chemical Reagent Factory. The Nafion was purchased from Sigma-Aldrich. Deionized water was used throughout this study.

Synthesis of Ti-BPDC-Pd: The Ti-BPDC was prepared according to the previously reported methods with modifications.[S1] In a 100 mL beaker, H_2BPDC (100 mg, 0.41 mmol) was dissolved in a mixed solution of DMF (30 mL) and acetic acid (1 mL) and sonicated for 10 min, before adding tetraethyl titanate (0.1 mL, 0.48 mmol). After 15 min of further sonication, the solution was transferred to a 100 mL Teflon-lined stainless-steel container and maintained at 150 °C for 72 h. The product was then collected by centrifugation, washed 3 times with DMF and methanol separately, and dried in a vacuum oven at 60 °C for 12 h. The powdered product (100 mg) was dispersed in 5.00 mL of deionized water and sonicated for 30 min to form a suspension. K_2PdCl_6 solution (10 mL) was then dropped into the suspension and stirred at 50 °C for 24 h. The solid product in the suspension was recovered by centrifugation, washed with deionized water and ethanol 5 times, and dried in a vacuum oven at 60 °C for 12 h. Ti-BPDC-M (M = Au, Ag, Pt, Cu, and Ni) were prepared by the same procedure.

Synthesis of PdO/TiO_2: Ti-BPDC-Pd is transferred into a ceramic boat and placed in a tube furnace. The sample is heated to 400 °C with a heating rate of 5 °C min^{-1} and keep at 400 °C for 8 h then naturally cooled to room temperature. The PdO/TiO_2 is obtained and can be directly used without further treatment. The loading ratio of Pd was changed by adjusting the amount of K_2PdCl_4 aqueous solution. The resulting sample was denoted as $xPdO/TiO_2$, where x represents the mass percentage of Pd (x = 0.5, 1, 2, 3). Metal/TiO_2 (M = Au, Ag, Pt, Cu, and Ni) were prepared by the same synthesis procedure. Specifically, the following metal salts were used as precursors: $HAuCl_4{\cdot}4H_2O$ for Au, $AgNO_3$ for Ag, $H_2PtCl_6{\cdot}xH_2O$ for Pt, $Cu(NO_3)_2{\cdot}3H_2O$ for Cu, $Ni(NO_3)_2{\cdot}6H_2O$ for Ni.

Synthesis of PdO/metal oxide: As a comparison, the reference compound PdO/P25 was prepared by utilizing P25 as the support to replace Ti-BPDC (considering that the Pd precursor cannot be adsorbed on P25 through chelation, the photodeposition method was adopted). Typically, 100 mg of P25 was dispersed in a mixture of water and ethanol (4/1, v/v) and injected with a certain amount of quantitative K_2PdCl_6 solution, and then fully sonicated for 10 min. The suspension was irradiated with a 300 W xenon lamp under a nitrogen atmosphere for 30 min. The resulting samples were washed with ethanol and dried at 60 °C overnight. The obtained solid sample followed the same calcination. The synthesis of other PdO/ZnO, PdO/CeO_2, and PdO/Al_2O_3 photocatalysts followed a similar procedure.

Photoactivity testing: The photocatalytic CH_4 conversion experiments were carried out in a CH_4 atmosphere (0.1 MPa) at room temperature in a 30 mL custom-made quartz tube reactor. In a typical test, 5 mg of catalyst was dispersed in 500 μL of DI water and then dropped onto a 1 × 5 cm clear glass and dried in air at 323 K. After the glass was vertically placed in the reactor, pure CH_4 was purged into the system. Afterward, the reactor was irradiated by an Xe lamp with a UV-vis light source. The incident light intensity was 200 mW cm^{-2} as measured by a photoradiometer (PL-MW2000, Beijing Perfectlight Technology Co., Ltd.). After the reaction, a gas chromatograph (Shimadzu GC-8A 2014C) equipped with a flame ionization detector (FID) and a thermal conductivity detector (TCD) was used for the determination of carbon oxide and H_2 in the reaction gas. Gas chromatography (Agilent 7820A) was used for the analysis of

CH_4, hydrocarbons, and CO_2 in the reaction gas. In isotope labeling experiments, the produced C_2H_6 was analyzed using gas chromatography-mass spectrometry (Shimadzu GC-MS QP 2020, Q-Exactive).

The apparent quantum yield (AQY) of C_2H_6 for the PdO/TiO_2 composite was measured with light irradiation. The photon flux of incident light was measured by a PL-MW200 photoradiometer (Beijing Perfectlight Co., Ltd.). The AQY was calculated according to the following equation:

$$AQY = \frac{N_e}{N_p} \times 100\% = \frac{2 \times M \times N_A \times h \times c}{S \times P \times t \times \lambda} \times 100\%$$

where N_e is the number of reaction electrons, N_p is the number of incident photons, M is the molar amount of C_2H_6, N_A is Avogadro constant, h is the Planck constant, c is the speed of light, S is the irradiation area, P is the light power density, t is the reaction time and λ is the incident light wavelength.

2. Characterizations

The morphology and elemental distribution of the samples were analyzed by field-emission scanning electron microscopy (FESEM) on the FEI Nova NANO-SEM 230 spectrophotometer and transmission electron microscopy (TEM), high-resolution TEM (HRTEM) and elemental mapping analysis using a JEOL 2100F instrument at an accelerating voltage of 200 kV. X-ray photoelectron spectroscopy (XPS) measurements were performed using a Thermo Scientific ESCA Lab250 spectrometer that consists of monochromatic Al Kα as the X-ray source, a hemispherical analyzer, and a sample stage with multiaxial adjustability to obtain the composition on the surface of the samples. All of the binding energies were calibrated using the C 1s peak of the surface adventitious carbon at 284.8 eV. The X-ray diffraction (XRD) patterns of the samples were measured on a Rigaku Miniflex diffractometer with Cu Kα radiation. Nitrogen adsorption-desorption measurements were performed on a Quantachrome Autosorb IQ instrument to measure the average diameter and specific surface area of the sample, using the Barrett-Joyner-Halenda (BJH) and Brunauer-Emmett-Teller (BET) methods, respectively. Free radical capture experiments were conducted on an electron paramagnetic resonance spectrometer (EPR, Bruker E500, Germany) by Shiyanjia Lab "www.shiyanjia.com". UV-vis diffuse reflectance spectroscopy (DRS) on UV-vis Spectrophotometers (Thermo Scientific Evolution 200 Series) was used to measure the optical properties of the samples with $BaSO_4$ as the internal reflectance standard. Temperature programmed desorption of CH_4 (CH_4-TPD) experiment was performed on a BelCata II apparatus. The photoelectrochemical analysis was conducted in a conventional three electrode cell with a Pt plate as the counter electrode and an Ag/AgCl electrode as the reference electrode. The working electrode was prepared on fluorine doped tin oxide (FTO) glass that was cleaned by sonication in ethanol and DI water and then dried at 60 °C for 3 h. The boundary of FTO glass was protected using Scotch tape. 5 mg sample was fully dispersed in 1 mL DMF and ethanol mix solvent by sonication to get a slurry. The slurry (15 μL) was spread onto the pre-treated FTO glass. The working electrode was dried at 80 °C for 1 h to improve adhesion. The exposed area of the working electrode was 0.25 cm^2. The electrochemical impedance spectroscopy (EIS) measurement was measured via an electrochemical workstation (MUTI AUTOLAB M204) in the three-electrode cell in the presence of 0.5 M KCl solution containing 5.0 mM $K_3[Fe(CN)_6]/K_4[Fe(CN)_6]$ by applying an AC voltage with 5 mV amplitude in a frequency range from 1 Hz to 100 kHz under open circuit potential conditions. The transient photocurrent density was measured in 0.2 M Na_2SO_4

aqueous solution (pH = 7) under light irradiation. The photoluminescence (PL) spectra for samples were analyzed on an Edinburgh Analytical Instrument F900 spectrophotometer with an excitation wavelength of 320 nm. The electron paramagnetic resonance (EPR) signal of the radical spin-trapped by DMPO was measured on a Bruker EPR A300 spectrometer. The Fourier transform-infrared (FT-IR) spectra were recorded on a Thermo IS-50 FTIR spectrometer. A 300 W Xe lamp (PLS-SXE 300D, Beijing Perfectlight Technology Co., Ltd.) was used as the irradiation source.

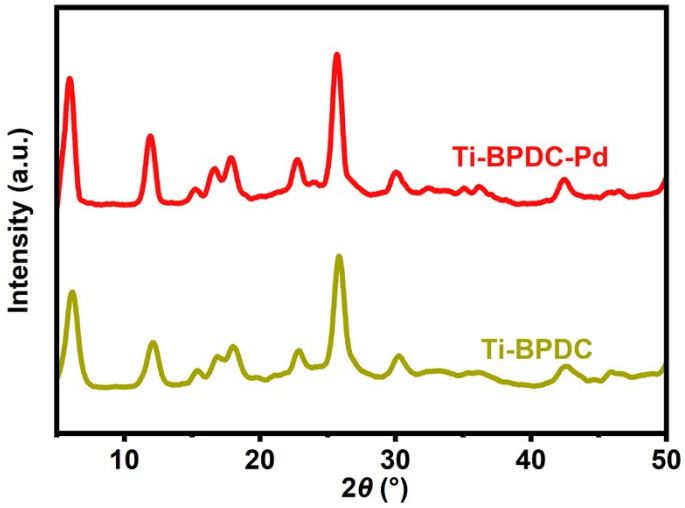

Fig. S1. X-ray diffraction (XRD) patterns of Ti-BPDC and Ti-BPDC-Pd.

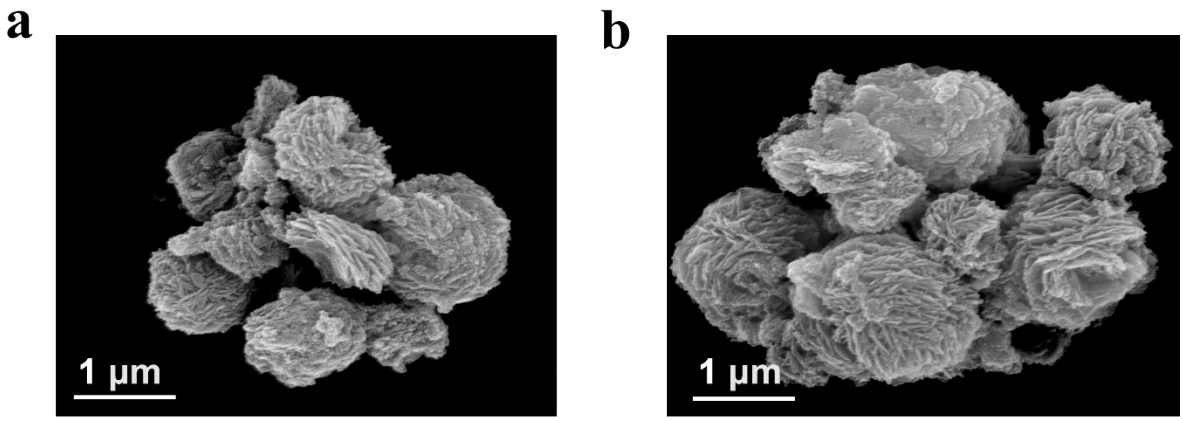

Fig. S2. SEM images of a) Ti-BPDC and b) Ti-BPDC-Pd.

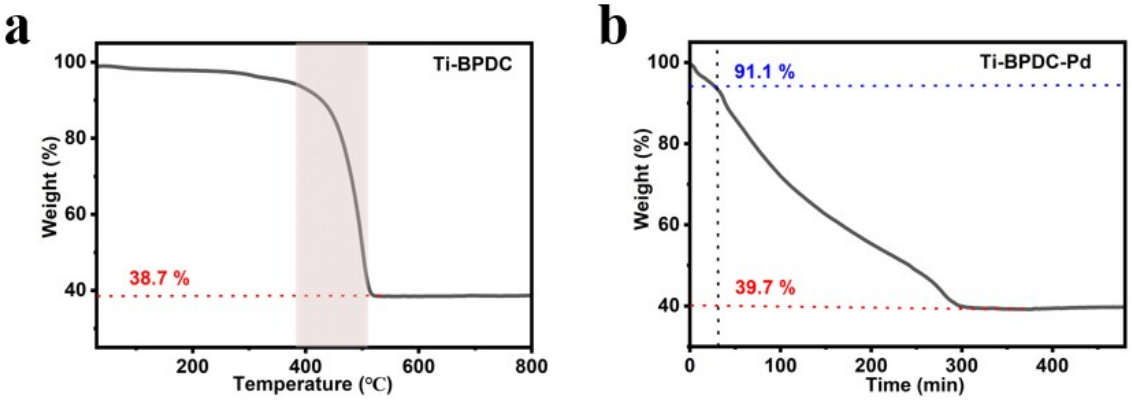

Fig. S3. a) Thermogravimetric (TG) analysis curve of Ti-BPDC in air with heating rate of 10 ℃/min and b) TG curve of Ti-BPDC-Pd.

Note: Ti-BPDC has a weight loss step at 380 to 500 ℃, and in order to better reconstruct the surface, 400 ℃ is selected for calcination. Additionally, the mass of Ti-BPDC-Pd is no longer changed after heat treatment at 400 ℃ for 6 h, and in order to remove C and N elements, the time is extended to 8 h to obtain a completely decomposed sample.

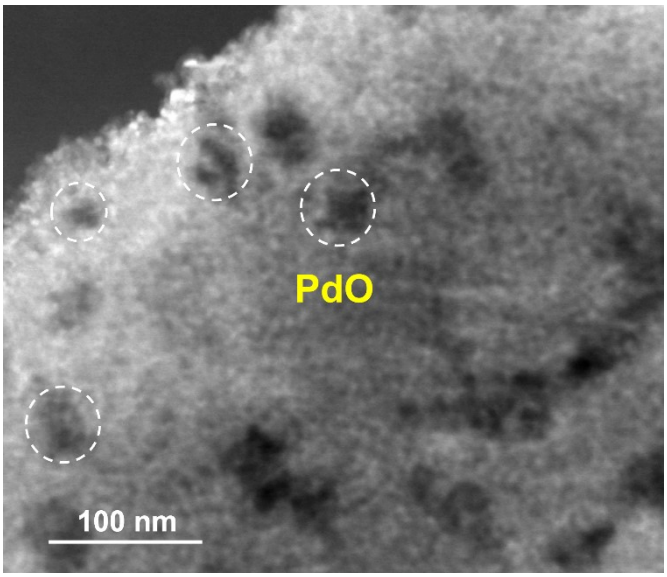

Fig. S4. TEM images of PdO/TiO_2.

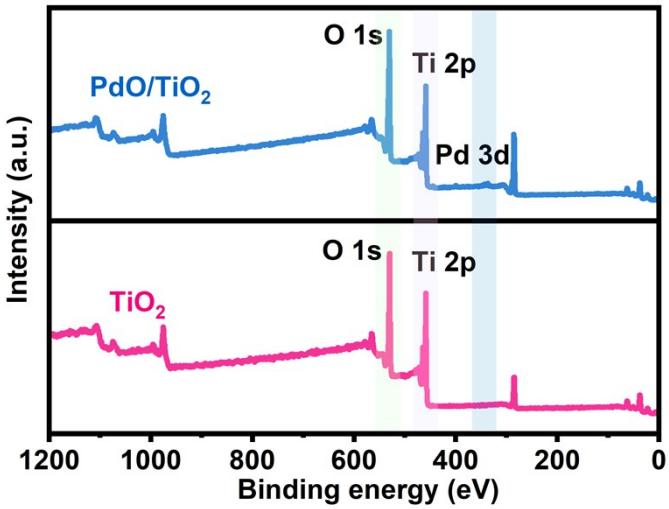

Fig. S5. X-ray photoelectron spectroscopy (XPS) survey spectra of PdO/TiO_2 and TiO_2.

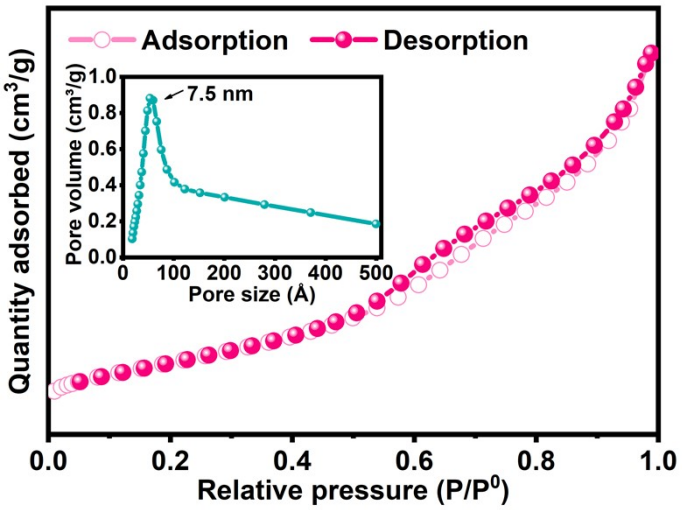

Fig. S6. Nitrogen adsorption-desorption isotherms of TiO_2 (inset: pore size distribution of TiO_2).

Table S1. Specific surface area and pore properties of catalysts.

Catalyst	Specific surface area (m^2/g)	Average pore size (nm)	Total pore volume (cm^3/g)
Pd/TiO_2	240.1	8.7	0.52
TiO_2	305.9	7.5	0.58

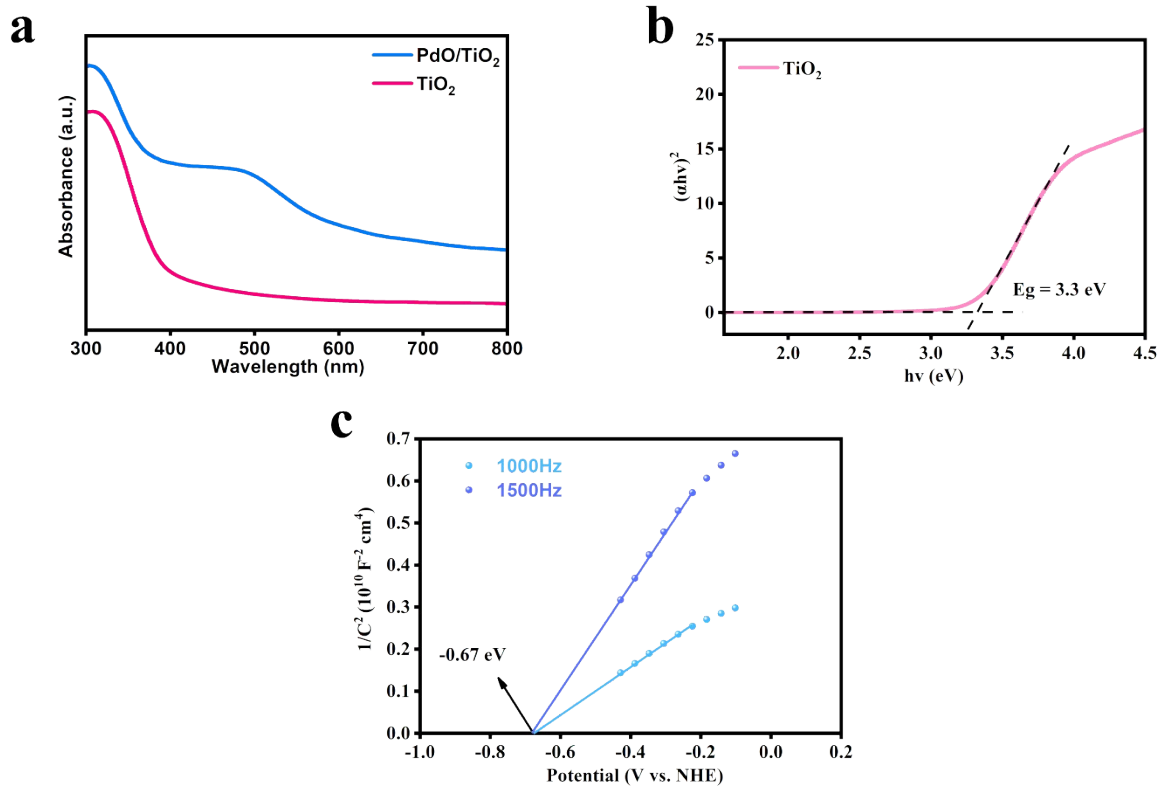

Fig. S7. a) DRS spectra of TiO_2 and PdO/TiO_2. b) Tauc plot for optical-band-gap determination of TiO_2. c) Mott-Schottky plot for TiO_2 in a 0.2 M Na_2SO_4 aqueous solution (pH = 7).

Note: To calculate the band gap energy, the following formula is used:

$$(\alpha h\nu)^2 = K\cdot(h\nu - Eg)$$

where α is the absorption coefficient, hν is the photon energy, K is a constant, and Eg is the band gap energy. As shown in Fig. S7b, the band gap of TiO_2 is evaluated to be 3.3 eV. In addition, the flat band position which refers to the conduction band (CB) of TiO_2 is estimated at −0.67 V vs. normal hydrogen electrode (NHE) according to the Mott-Schottky analysis (Fig. S7c). The valence band (VB) of TiO_2 is then calculated with the value of 2.83 V vs. NHE.

Table S2. Inductively coupled plasma atomic emission spectrometry (ICP-AES) analysis results for all composite samples.

Catalyst	Pd (wt.%)
0.5PdO/TiO_2	0.48
1PdO/TiO_2	1.02
2PdO/TiO_2	1.95
3PdO/TiO_2	2.87

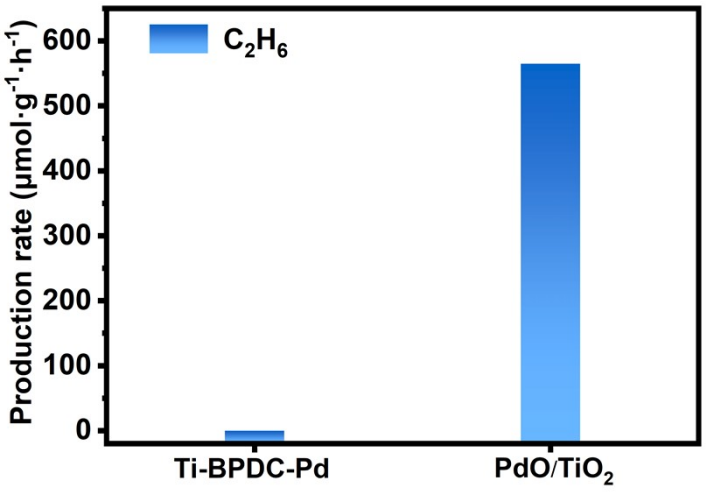

Fig. S8. Photocatalytic NOCM performance over MOF precursor (Ti-BPDC-Pd) and PdO/TiO_2.

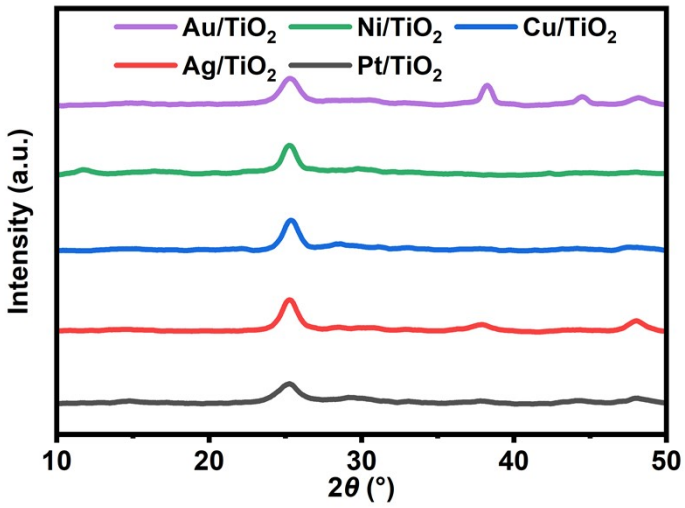

Fig. S9. XRD patterns of different metal-modified TiO_2 samples.

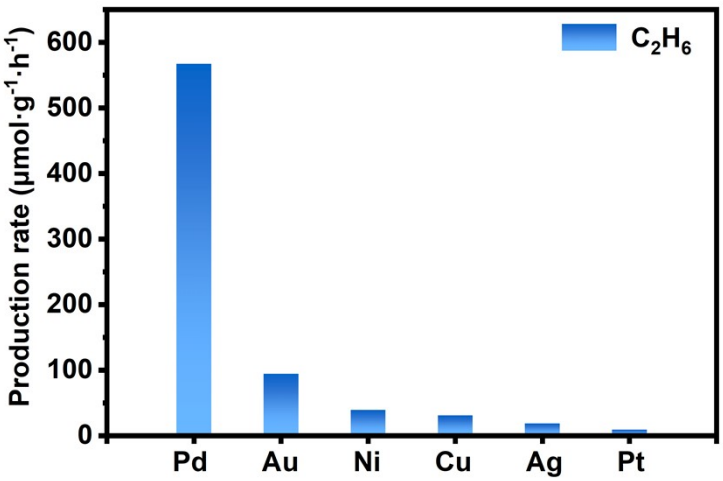

Fig. S10. Photocatalytic NOCM performance over different metal-modified TiO_2 samples.

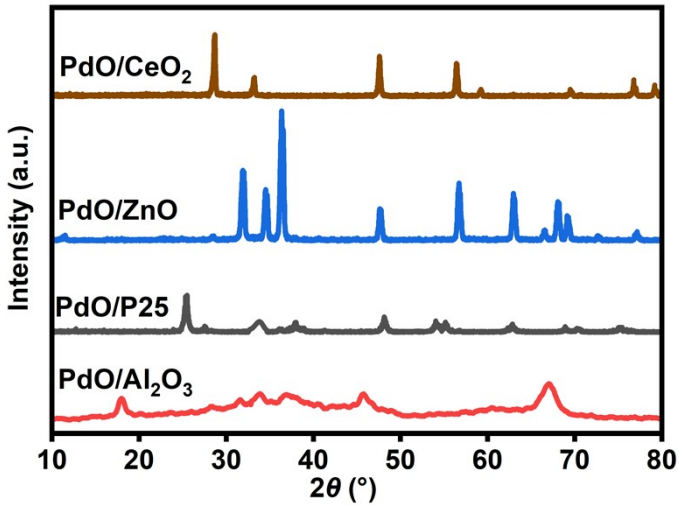

Fig. S11. XRD patterns of PdO-supported oxide substrates.

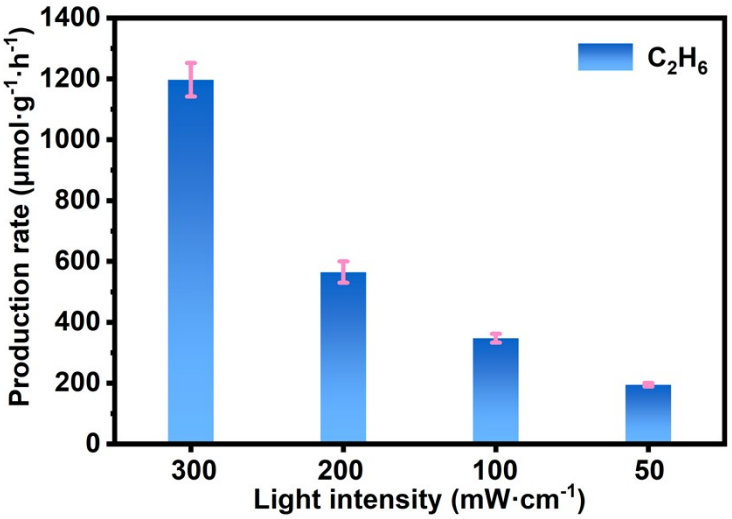

Fig. S12. Light intensity-dependent photocatalytic NOCM over PdO/TiO_2.

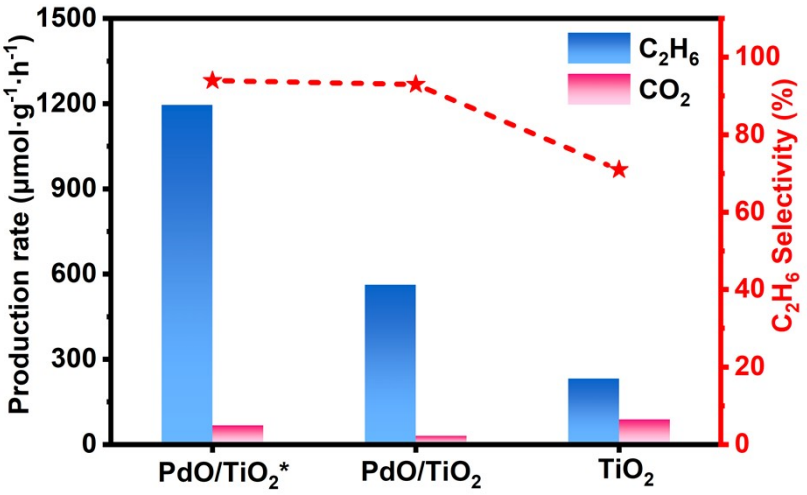

Fig. S13. The production rate of carbonaceous products in photocatalytic NOCM after 4 h light irradiation.
Note: * indicates that the reaction condition is irradiation at a light intensity of 300 mW·cm^{-2}.

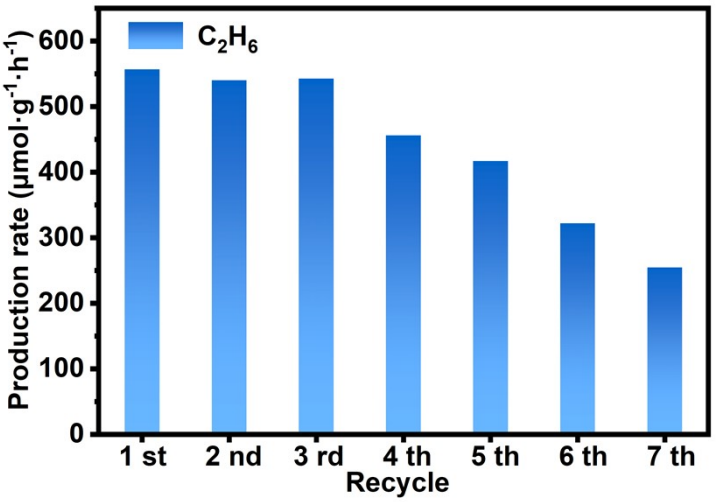

Fig. S14. Rate of C_2H_6 in the cyclic tests by PdO/TiO_2 without regeneration treatment. Each cycle lasts 4 h.

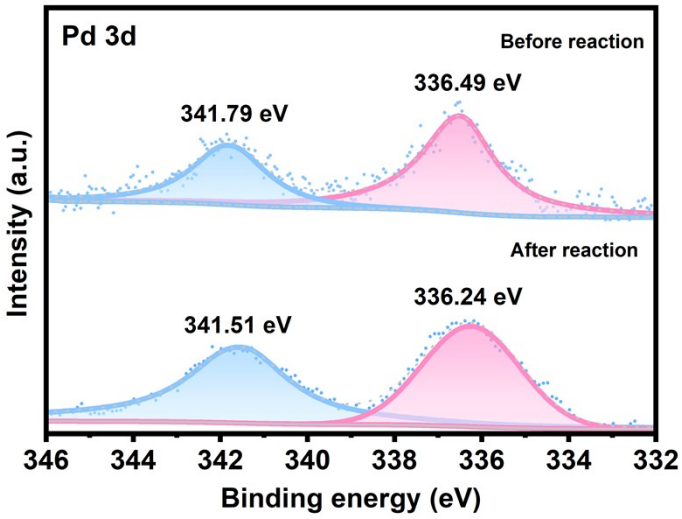

Fig. S15. High-resolution XPS spectrum of Pd 3d in PdO/TiO_2 before and after reaction.

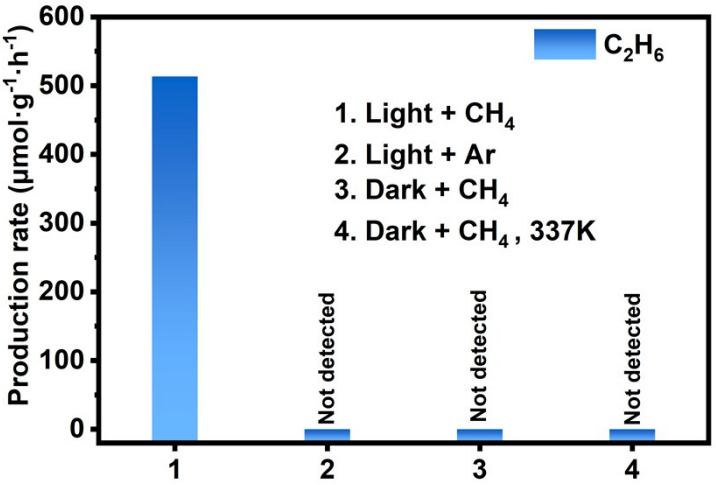

Fig. S16. The comparison of NOCM performance over PdO/TiO_2 in control experiments.

Table S3. Representative works on photocatalytic nonoxidative coupling of CH_4 to C_2H_6.

Entry	Catalyst	Reaction conditions	C_2H_6 production rate	Ref
1	PdO/TiO_2	300 W Xe lamp; 5 mg catalyst; 0.1 MPa CH_4	1196 μmol g^{-1} h^{-1}, selectivity: 94%	**This work**
2	Pd_1/TiO_2	300 W Xe lamp; 3 mg catalyst; 0.1 MPa CH_4	910 μmol g^{-1} h^{-1}, selectivity: 94%	S2
3	Au/ZnO	300 W Xe lamp; 10 mg catalyst; 0.1 MPa CH_4	1121 μmol g^{-1} h^{-1}, selectivity: 90%	S3
4	Pt SAs/TiO_2	300 W Xe lamp; 15 mg catalyst; 0.1 MPa CH_4	252 μmol g^{-1} h^{-1}, selectivity: 98%	S4
5	Ag-HPW/TiO_2	400 W Xe lamp; 0.1 g catalyst; 0.3 MPa CH_4	23 μmol g^{-1} h^{-1}, selectivity: 78%	S5
6	$Ag/NaTiO_3$	4*8 W 254nm UV lamp; 10 mg catalyst; 0.1 MPa CH_4	194 μmol g^{-1} h^{-1}, selectivity: 89%	S6
7	CeO_2@CZ	300 W Xe lamp; 30 mg catalyst; 300 μmol CH_4	52 μmol g^{-1} h^{-1}, selectivity: 98%	S7

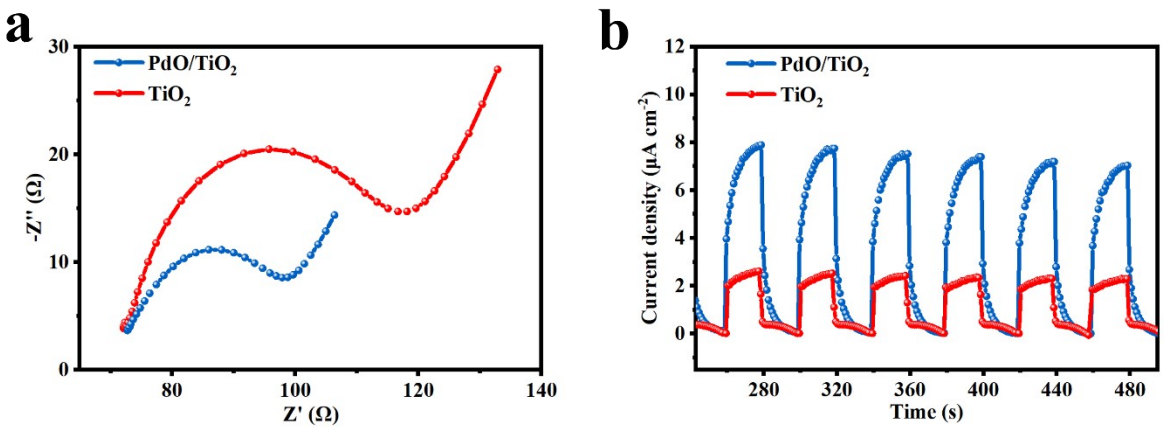

Fig. S17. a) EIS Nyquist plots and b) transient photocurrent spectra of PdO/TiO_2 and TiO_2.

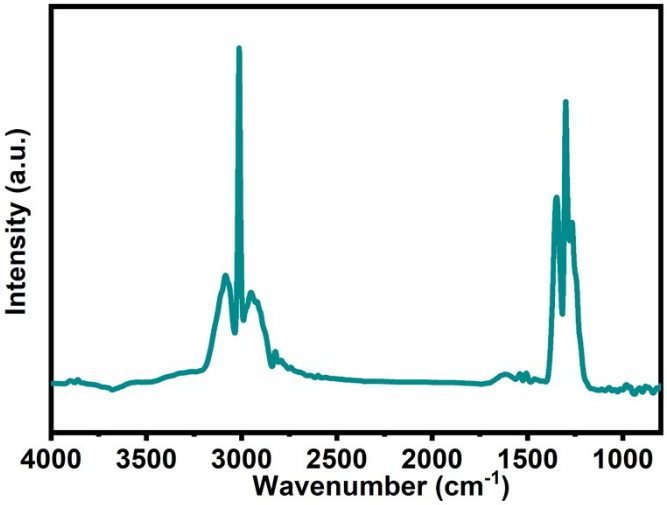

Fig. S18. In situ FTIR spectra for CH_4 adsorption over PdO/TiO_2.

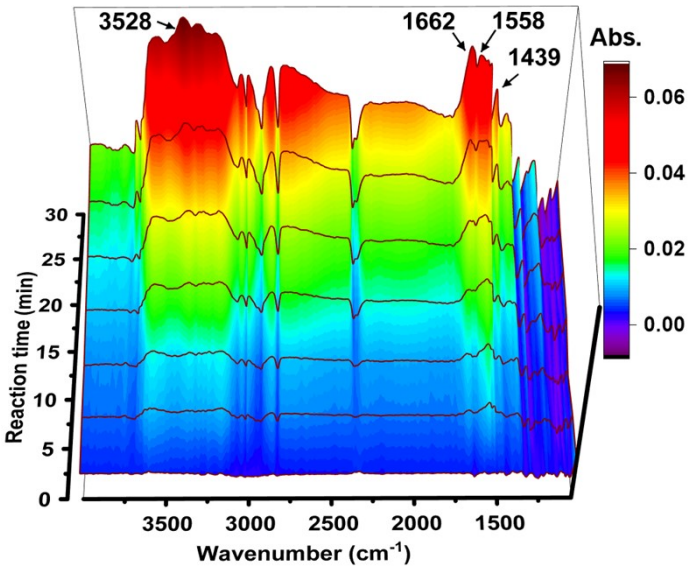

Fig. S19. In situ FTIR spectra for photocatalytic NOCM over TiO_2.

References

S1 X. Y. He, Y. J. Ding, Z. N. Huang, M. Liu, M. F. Chi, Z. L. Wu, C. Segre, C. S. Song, X. Wang, X. W. Guo, *Angew. Chem. Int. Ed.* **2023**, *62*, e202217439.

S2 W. Q. Zhang, C. F. Fu, J. X. Low, D. L. Duan, J. Ma, W. B. Jiang, Y. H. Chen, H. J. Liu, Z. M. Qi, R. Long, Y. F. Yao, X. B. Li, H. Zhang, Z. Liu, J. L. Yang, Z. G. Zou, Y. J. Xiong, *Nat. Commun.* **2022**, *13*, 2806.

S3 K. Zheng, X. J. Zhang, J. Hu, C. B. Xu, J. C. Zhu, J. Li, M. Y. Wu, S. Zhu, L. Li, S. M. Wang, Y. M. Lv, X. He, M. Zuo, C. Y. Liu, Y. Pan, J. F. Zhu, Y. F. Sun, Y. Xie, *Sci China Chem* **2023**, *67*, 869-875.

S4 P. Zhang, J. W. Li, H. W. Huang, X. Y. Sui, H. H. Zeng, H. J. Lu, Y. Wang, Y. Y. Jia, J. A. Steele, Y. H. Ao, M. B. J. Roeffaers, S. Dai, Z. Z. Zhang, L. Z. Wang, X. Z. Fu, J. L. Long, *J. Am. Chem. Soc.* **2024**, *146*, 24150-24157.

S5 X. Yu, V. L. Zholobenko, S. Moldovan, D. Hu, D. Wu, V. V. Ordomsky, A. Y. Khodakov, *Nat. Energy* **2020**, *5*, 511-519

S6 J. J. Zhang, J. N. Shen, D. M. Li, J. L. Long, X. C. Gao, W. H. Feng, S. Y. Zhang, Z. Z. Zhang, X. X. Wang, W. M. Yang, *ACS Catal.* **2023**, *13*, 2904-2105.

S7 G. M. Wang, X. W. Mu, R. K. Tan, Z. Y. Pan, J. Y. Li, Q. Y. Zhan, R. Fu, S. Y. Song, L. Li, *ACS Catal.* **2023**, *13*, 11666-11674.